Macromolecules

pubs.acs.org/Macromolecules Article

Physically Cross-Linked Polybutadiene by Quadruple Hydrogen Bonding through Side-Chain Incorporation of Ureidopyrimidinone with Branched Alkyl Side Chains

Jente Verjans, Alexis André, Evelyne Van Ruymbeke, and Richard Hoogenboom*

Cite This: *Macromolecules* 2022, 55, 928−941 Read Online

ACCESS | Metrics & More | Article Recommendations | Supporting Information

ABSTRACT: The synthesis of a supramolecular polymer network based on ureidopyrimidinone (UPy) is demonstrated starting from a low-molecular weight polybutadiene (PB) polymer, which was modified with UPy quadruple hydrogen-bonding motifs through UV-initiated thiol−ene chemistry under ambient conditions. Here, the UPy units contain a branched alkyl side chain rather than a methyl group, as is the case in most literature examples. The sterically demanding aliphatic 2-ethylpentyl side chain was introduced to prevent stacking of the UPy dimers and to enhance the compatibility of the UPy unit with the apolar PB polymer matrix. The UPy units were grafted onto PB with different functionalization degrees yielding materials with a relatively broad range of glass transition temperatures (T_g) and material properties, as evaluated by thermogravimetric analysis, differential scanning calorimetry (DSC), and dynamic mechanical thermoanalysis. Importantly, only the system with 13 mol % UPy functionalization showed some macroscopic phase separation as indicated by its partial opaque appearance, even though this was not detected by DSC. Previous reports on PB end functionalized with methyl-functional UPy revealed phase separation through DSC, indicating that the branched side chains indeed suppress the phase separation. The network dynamics were assessed by rheological measurements at different temperatures, which were subsequently fitted to the sticky Rouse model and creep experiments. We found that the sticky Rouse model satisfactorily fits the linear response of the systems in the terminal regime. However, significant discrepancy from theory still persists in the rubbery plateau regime. This deviation is attributed to the presence of structural defects in the systems. Altogether, this work demonstrates the importance of designing the supramolecular physical cross-linker unit with a branched aliphatic side chain to enhance the compatibility with the polymer matrix for the formation of supramolecular polymer networks.

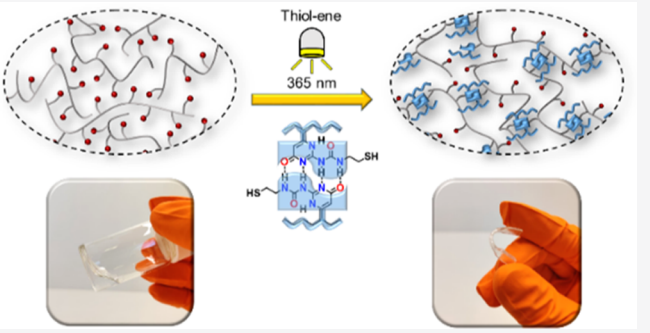

INTRODUCTION

Over the past century, polymer materials have become an established part of our daily lives by their prevalence in a wide variety of applications, ranging from simple consumer goods to highly advanced engineering and biomedical systems. However, the majority of these systems still consist of static materials with limited responsive properties. Inspired by nature, supramolecular chemistry has profoundly influenced the design of polymers toward smart materials. The introduction of non-covalent interactions in conventional polymers enables the production of dynamic materials, which respond to external triggers like pH,[1,2] light,[3,4] and temperature.[5,6] Fueled by the large variety of non-covalent interactions available to form intermolecular connections between polymers, supramolecular polymer networks can be designed with tailored properties for various application domains ranging from electronics[7] over bulk materials[8] to medicine.[9] The key types of supramolecular interactions include hydrophobic interactions,[10,11] $\pi-\pi$ stacking,[12,13] host−guest interactions,[14−16] metal−ligand complexation,[17−19] electrostatic interactions,[20−22] and hydrogen bonding.[23,24] From the formerly mentioned interactions, hydrogen bonding provides an excellent platform for the development of dynamic materials.[24] Although a single hydrogen bond is intrinsically weak, the combined strength of multiple hydrogen bonds can have a powerful effect. This is beautifully illustrated by the supramolecular rubber designed by Leibler and co-workers, where multitopic small molecular compounds derived from fatty diacids and triacids bearing an amide and urea-based functionalities resulted in a supramolecular material with self-healing behavior at room temperature.[25] Although low-molecular weight building blocks help to decrease the melt viscosity and consequently improve the processability, the

Received: September 9, 2021
Revised: January 4, 2022
Published: January 19, 2022

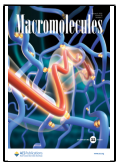

https://doi.org/10.1021/acs.macromol.1c01908
Macromolecules 2022, 55, 928−941

mechanical performance of these materials is rather limited.[26] To enhance the mechanical properties, polymer precursors and multiple hydrogen-bonding arrays can be used. A key event in supramolecular chemistry was the development of the quadruple hydrogen-bonding array ureidopyrimidinone (UPy) by Meijer and co-workers.[27] The strong association constant combined with self-complementarity and facile synthesis has made it an attractive building block in designing new hydrogen-bonded polymer networks, both in the context of bulk materials and polymers for biological applications.[23,28−30]

However, in most UPy-related polymer materials, a methyl side chain resulting from the readily accessible 6-methyl isocytosine is used (Me-UPy). The high polarity of this UPy derivative tends to cause phase separation in apolar polymer matrices by $\pi-\pi$ stacking of the UPy dimers especially when combined with urethane or urea bonds between the polymer and the UPy moieties.[31−37] Mather et al.[31] reported Me-UPy end-functionalized linear and star-shaped poly(ethylene-*co*-propylene) materials where microphase-separated morphologies were detected with small angle X-ray scattering and atomic force microscopy (AFM), while Botterhuis and co-workers[32] synthesized telechelic Me-UPy polydimethylsiloxanes showing microphase separation evidenced by the presence of a characteristic melting peak in differential scanning calorimetry (DSC) and the visualization of nanofibers in AFM. Oscillatory shear rheology complemented the DSC and AFM results by strengthening the hypothesis that the fiber-like structures were indeed present throughout the bulk rather than exclusively on the surface. Recently, Kan et al. reported UPy end-functional poly(ethylene-*co*-butylene) polymers where the UPy side chain was varied from a methyl to an *n*-octyl substituent.[36] For the methyl variant, phase separation was observed in both AFM and DSC measurements, which was attributed to the formation of nanofibers by stacking of UPy dimers. When increasing the steric hindrance on the UPy units, the nanofibers disappeared in the resulting supramolecular polymer materials, effectively demonstrating the impact of the UPy side chain on the morphology and mechanical properties in UPy-based supramolecular materials.

Although the previous work mainly encompassed chain end-functional UPy polymers, it seemed interesting to transfer this methodology to side chain-functional supramolecular polymer networks with apolar polymer precursors. In this work, it is hypothesized that appropriate adaptation of the UPy side chain could suppress potential phase separation in two ways, that is, by increasing the compatibility with the polymer matrix and by introducing sterical hindrance to prevent stacking of the UPy dimers. Therefore, we chose a UPy motif with a branched alkyl group, which was first introduced to enhance the solubility of the UPy units, allowing application of ambient reaction conditions for the synthesis of the materials.[34,38] To demonstrate our hypothesis, we opted for commercially available 1,2-polybutadiene (PB) as a polymer platform because the apolar polymer matrix enforces the hydrogen bonds, and the large abundance of vinyl side chains allows facile variation in the functionalization degree via thiol−ene chemistry. In this way, we anticipate to gain more insights into the application of a UPy unit with a branched alkyl side chain in supramolecular polymer materials based on PB with UPy in the side chain. First, the synthesis of the hydrogen-bonding units will be discussed, followed by the synthesis and characterization of the supramolecular polymer networks. To achieve physical cross-linking of the polymers, synthetic pathways were designed to incorporate a functional handle onto the H-bonding units compatible with the side chains of the polymer. We chose for photo-initiated radical thiol−ene chemistry because of the facile application and mild reaction conditions.[39] A commercially available PB comprising vinyl side chains was combined with a quadruple H-bonding UPy unit functionalized with a thiol group. In the first part of the paper, the synthesis of the UPy with a terminal thiol and its use for functionalization of PB will be discussed. Next, the structural characterization of the resulting polymers and their thermal and mechanical properties will be described. The last part of this work focuses on the fitting of the data with the sticky Rouse model to gain further insights into the dynamic network properties.

EXPERIMENTAL SECTION

Materials. Unless stated otherwise, all reagents were obtained from commercial sources and used without further purification. All high-performance liquid chromatography grade solvents were purchased from Sigma-Aldrich [acetonitrile (ACN), chloroform ($CHCl_3$), diethyl ether (Et_2O), methanol (MeOH), dichloromethane (DCM), ethyl acetate (EtOAc), triethylamine (Et_3N), and tetrahydrofuran (THF)], Biosolve (*N*,*N*-dimethylformamide), or Fisher Scientific (toluene). Dry ACN, Et_3N, and THF were obtained from a custom-made JW Meyer solvent purification system and dried over aluminum oxide columns. Argon (Ar) (Alphagaz 1) was purchased from Air Liquide and used as supplied. Magnesium sulfate ($MgSO_4$), sodium chloride (NaCl), sodium bicarbonate ($NaHCO_3$), hydrochloric acid (HCl) (37% in water), and guanidine carbonate (99%) were purchased from Fisher Scientific. PB [vinyl content: 89%, M_w = 4.0 kg/mol, $Đ$ = 1.39, measured by THF−size-exclusion chromatography (SEC) relative to polystyrene standards] was purchased from Sigma-Aldrich. 2-Ethylhexanoyl chloride (98%), monoethyl potassium malonate (98%), and 1,1′-carbonyldiimidazole (CDI) (97%) were purchased from TCI Chemicals. Magnesium chloride ($MgCl_2$) (98%) and 2,2-dimethoxy-2-phenylacetophenone (DMPA) (98%) were purchased from Acros Organics. Trifluoroacetic acid (TFA) (99.5%) was purchased from Biosolve. 6-(2-Ethylpentyl)imidazolide was synthesized according to a literature procedure.[38]

Equipment. ^{1}H nuclear magnetic resonance (^{1}H NMR) spectra were recorded on a Bruker Avance 300 Ultrashield or Bruker ADVANCE II 400 MHz spectrometer at room temperature. The compounds were dissolved in either chloroform-*d* or dimethylsulfoxide-d_6 (DMSO-d_6) from Euriso-top. The chemical shifts (δ) are given in parts per million (ppm) and referenced against the residual $CHCl_3$ and DMSO signals at 7.26 and 2.50 ppm, respectively. SEC was performed on a Varian PL-GPC 50 Plus system using THF at 1 mL/min as the eluent and equipped with two PLgel 5 μm MIXED-D columns, a PL-AS RT autosampler, and RI detector. Molecular weights were determined with the RI detector using polystyrene standards. Liquid chromatography−mass spectrometry (LC−MS) spectra were acquired on a quadrupole ion trap LC mass spectrometer (Thermo Finnigan MAT LCQ mass spectrometer) equipped with electrospray ionization. Centrifugation was performed on an ALC multispeed refrigerated centrifuge PK 121R from Thermo Scientific using 50 mL centrifuging tubes with screw caps from VWR or 15 mL high-clarity polypropylene conical tubes from Falcon. Thermogravimetric analysis (TGA) was performed with a Mettler Toledo TGA/SDTA851e instrument under a nitrogen atmosphere at a heating rate of 10 °C/min from 25 to 800 °C. DSC analyses were performed with a Mettler Toledo instrument 1/700 under a nitrogen atmosphere at a heating rate of 10 °C/min. Dynamic mechanical thermoanalysis (DMTA) was performed on a Mettler Toledo DMA/SDTA861e using the shear mode on 8 mm disks. The temperature was increased from −50 to 150 °C at a heating rate of 3 °C/min. Rheological experiments were measured on an Anton Paar MCR 302 rheometer equipped with a CTD 450 oven using a parallel plate geometry and 8

https://doi.org/10.1021/acs.macromol.1c01908
Macromolecules 2022, 55, 928−941

Scheme 1. Synthetic Scheme for the Synthesis of UP-SH[a]

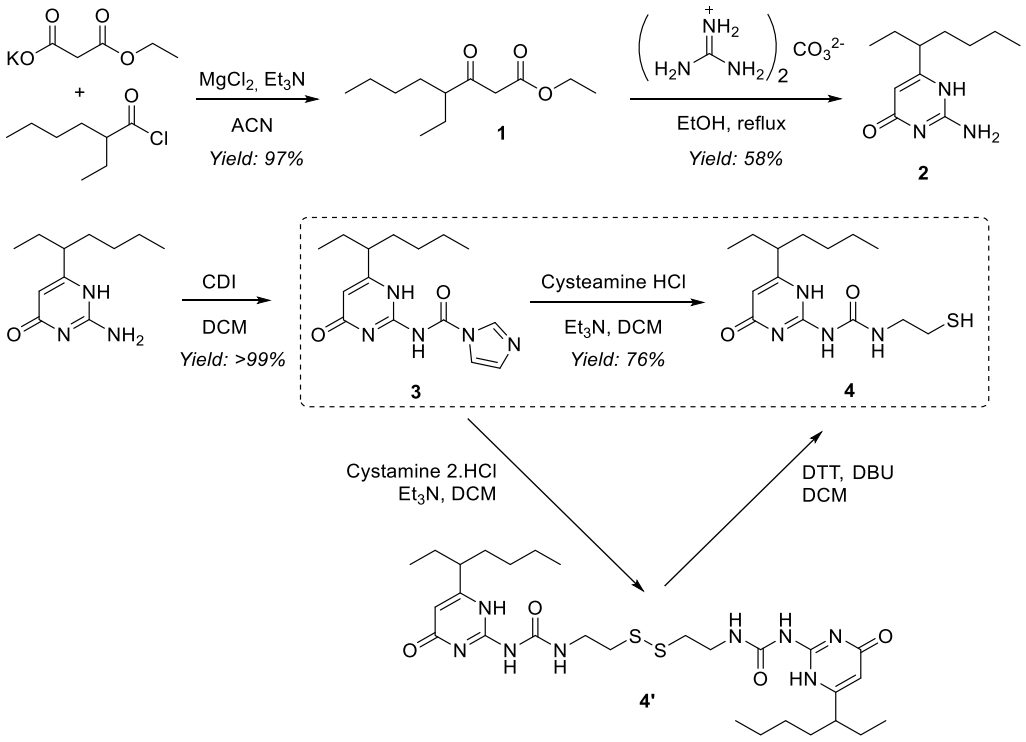

[a]Top: synthesis of isocytosine core 2; bottom: synthesis of UPy-SH 4.

mm disk samples. Unless specified otherwise, the experiments were performed using a normal force of 1 N, an angular frequency of 10 rad/s, and a strain of 0.1%. Amplitude sweeps were performed from 0.1 to 100% with a constant angular frequency of 10 rad/s. Frequency sweeps were carried out with an angular frequency ranging from 600 to 0.001 rad/s at constant temperature, and the measurement was stopped when a crossover of the storage and loss modulus (G' and G'', respectively) appeared. Creep recovery experiments were performed using a stress alternating between 0 and 2000 Pa. In a typical test, a stress of 2000 Pa was applied for 300 s, followed by a 100 s recovery period, and the corresponding strain profile was recorded over time.

Methods. *Synthesis of Ethyl 4-Ethyl-3-oxooctanoate.*[40] Monoethyl potassium malonate (109.9 g, 0.65 mol, 2.1 equiv) was dissolved in dry ACN (940 mL). The solution was cooled with an ice bath followed by addition of dry Et_3N (140 mL) and $MgCl_2$ (73.2 g, 0.77 mol, 2.5 equiv). The resulting slurry was stirred at room temperature for 2.5 h. The slurry was again cooled with an ice bath, and 2-ethylhexanoyl chloride (53.25 mL, 0.31 mol, 1 equiv) was added dropwise through an addition funnel. The slurry was allowed to warm up to room temperature overnight while stirring. The solvent was removed under reduced pressure, toluene (500 mL) was added, and the resulting solution was concentrated under reduced pressure. After addition of another portion of toluene (500 mL), the solution was cooled with an ice bath, and an aqueous solution of 13% HCl (427 mL) was carefully added. The aqueous layer was separated, and the organic layer was washed with an aqueous solution of 12% HCl (2 × 110 mL) and water (1 × 110 mL), dried over $MgSO_4$, and the solvent was removed under reduced pressure. The product was obtained as a yellow oil (yield: 63.89 g, 97%). ^{1}H NMR analysis indicated that the product was a mixture of the keto (73%) and enol (27%) tautomers. ^{1}H NMR (400 MHz, chloroform-*d*): δ enol: 12.09 (s, 1H), 4.96 (s, 1H), 2.00−1.90 (m, 1H); keto: 4.19 (q, J = 7.1 Hz, 1H), 3.44 (s, 2H), 2.50 (tt, J = 7.8, 5.7 Hz, 1H), 1.72−1.16 (m, 12H), 0.92−0.84 (m, 6H).

Synthesis of 6-(2-Ethylpentyl)isocytosine.[38] Guanidine carbonate (60.69 g, 0.337 mol, 1.13 equiv) and ethyl 4-ethyl-3-oxooctanoate (63.89 g, 0.298 mol, 1 equiv) were dissolved in ethanol (520 mL), and the resulting mixture was refluxed overnight. The solvent was removed under reduced pressure. The crude product was redissolved in chloroform (500 mL) and washed with a saturated aqueous solution of $NaHCO_3$ (2 × 250 mL) and brine (1 × 250 mL). Drying over $MgSO_4$ and removal of the solvent yielded the product as a pale yellow powder (yield: 36.48 g, 58%). ^{1}H NMR (400 MHz, chloroform-*d*): δ 6.52 (s, 2H), 5.60 (s, 1H), 2.25−2.13 (m, 1H), 1.62−1.46 (m, 4H), 1.34−1.13 (m, 4H), 0.91−0.77 (m, 6H).

Synthesis of 2-Mercaptoethylureido-6-(2-ethylpentyl)-pyrimidone (UPy-SH). 6-(2-Ethylpentyl)isocytosine (10.13 g, 48.4 mmol, 1 equiv) and CDI (10.43 g, 64.4 mmol, 1.33 equiv) were dissolved in dry DCM (51 mL), and the yellow solution was stirred overnight at room temperature under an inert atmosphere. The solution was diluted with DCM (175 mL) and washed with water (1 × 50 mL) and brine (1 × 50 mL) and dried over $MgSO_4$. The solvent was removed under reduced pressure, and the product was used in the next step without further purification.

The obtained 6-(2-ethylpentyl)imidazolide (14.68 g, 48.4 mmol) was dissolved in dry DCM (70 mL), cysteamine HCl (6.74, 59.3 mmol, 1.2 equiv) and triethyl amine (8.5 mL, 1.2 equiv) were added, and the dark orange solution was stirred at room temperature overnight. The reaction mixture was diluted with DCM (70 mL) and washed with 1 M HCl solution (1 × 50 mL), saturated $NaHCO_3$ solution (1 × 50 mL), and brine (1 × 50 mL), dried with $MgSO_4$, and evaporated under reduced pressure. The product was further purified *via* column chromatography (silica, gradient 1 to 2% methanol in chloroform), resulting in a light yellow oil, which crystallized to a white solid over time (yield: 11.73 g, 76%). ^{1}H NMR (300 MHz, chloroform-*d*): δ 13.12 (s, 1H), 11.99 (s, 1H), 10.49 (s, 1H), 5.82 (s, 1H), 3.47 (td, J = 7.5, 7.0, 5.5 Hz, 2H), 2.74 (dt, J = 8.1, 7.0 Hz, 2H), 2.31 (ddd, J = 9.0, 5.6, 3.5 Hz, 1H), 1.83−1.43 (m, 5H), 1.40−1.14 (m, 4H), 0.88 (m, 6H).

General Procedure of Grafting UPy-SH onto PB via Thiol−Ene Chemistry. 1,2-Polybutadiene (3−4 wt %) and UPy-SH (5−15 mol % to total vinyl bonds) were dissolved in dry THF and degassed by argon bubbling (30 min). DMPA (10 mol % to thiol) was dissolved in dry THF and added to the solution, which was irradiated by UV light

https://doi.org/10.1021/acs.macromol.1c01908
Macromolecules 2022, 55, 928−941

(365 nm) for 2.5 h at room temperature. The solvent was partially evaporated, and the polymer was precipitated in cold methanol (5% UPy) or cold diethyl ether (7−15% UPy).

RESULTS AND DISCUSSION

The synthesis of the isocytosine core of the UPy is modular with respect to the side chain. By preparing the corresponding β-keto ester, a custom isocytosine can be synthesized following previous literature reports.[40,41] Eventually, the desired UPy molecules can be obtained in a two-step procedure by generating an activated isocytosine, which readily reacts with a primary amine bearing the desired functional handle (Scheme 1).[38]

Compounds **1** to **3** were synthesized according to literature protocols.[38,40] The synthesis of target compound **4** has already been published following a different pathway where disulfide **4′** was synthesized.[42] By coupling **3** to cystamine (the disulfide form of cysteamine), bisUPy **4′** was formed, and reduction of the disulfide was necessary to obtain the thiol. Additionally, an excess of **3** was needed to increase the conversion. To avoid this extra reduction step and reduce the consumption of isocytosine **2**, we attempted to directly use cysteamine for preparing thiol-functionalized UPy **4** (dashed box in Scheme 1).

However, a small amount of disulfide formation was observed in the proton nuclear magnetic resonance (^{1}H NMR) spectra after the initial workup (signal *j′* and *k′* in Figure 1), potentially induced by the sodium bicarbonate

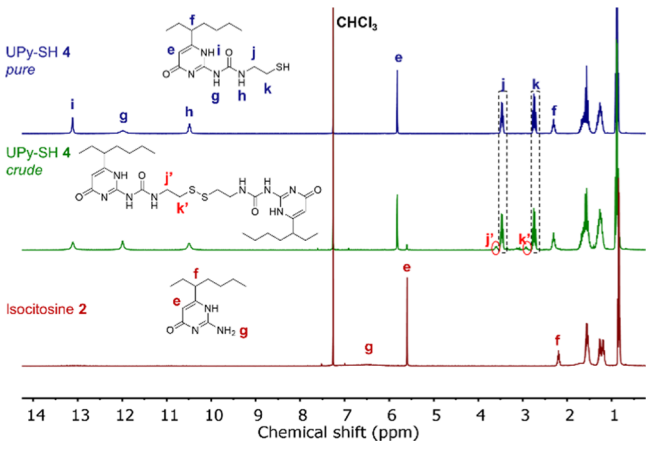

Figure 1. ^{1}H NMR spectra of purified compound **2** and compound **4** before and after purification.

washing step. Nonetheless, purification by column chromatography enabled isolation of most of the pure target compound, while additional UPy-SH could still be recovered from the impure part containing the disulfide side product after reduction of the disulfide with dithiothreitol (DTT).

After synthesizing the UPy units, the functionalized polymers were prepared in solution via photoinitiated radical thiol−ene coupling. We selected 1,2-PB as a polymer platform because the abundant vinyl side chains allow a large range in the degree of functionalization (DF), and it is commercially available as a viscous liquid in a low-molecular weight form, as seen in Figure 2. This low molar mass and absence of significant chain entanglements allow a better understanding of the changes in mechanical properties induced by subsequent physical cross-linking. The amount of vinyl side chains (89%)

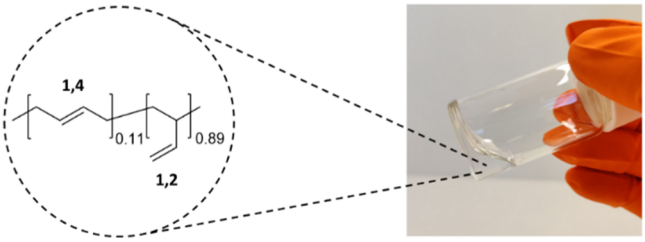

Figure 2. Molecular structure of the utilized 1,2-(PB) and physical representation of its viscous behavior.

and main-chain alkene bonds (11%) was determined with ^{1}H NMR spectroscopy.[43]

However, the close proximity of the vinyl groups can also cause intramolecular cyclization reactions when radicals are present, as illustrated in Scheme 2. Consequently, this limits the overall thiol conversion when full functionalization of the polymer is targeted. Although we only aimed for partial functionalization, which is less affected by these minor side reactions due to the lower radical concentrations, a small part of the vinyl side chains might still be consumed in cyclization reactions.[44−48] Nonetheless, the decreased thermal energy of photoinitiation at room temperature should repress these cyclization reactions, as the activation energy of cyclization is slightly higher than that of thiyl addition.[46]

Importantly, these side-chain vinyl units (formed by 1,2-addition of 1,3-butadiene during polymerization) were found to have superior reactivity relative to the alkenes in the main chain (from 1,4-addition), and no specific evidence was found that the 1,4-alkenes take part in cyclization side reactions in a significant manner.[49−51] In fact, the random distribution of 1,4-alkenes in the polymer main chain was reported to even decrease the cyclization reactions of the 1,2-vinyl side chains.[44] Therefore, the internal 1,4-alkenes were used as an internal standard for calculation of the DF, as sub-stoichiometric functionalization was found to lead to an almost exclusive reaction with the more reactive 1,2-vinyl units, which was also previously used by Lotti et al. for thiol−ene functionalization of the same PB polymer.[47] This method for the determination of DF is only based on comparison of the integrals of specific signals of the 1,4-alkenes and the UPy side chains, and, hence, the occurrence of minor cyclization reactions of the 1,2-vinyl units will not interfere with this determination of the DF. The incorporation of UPy was evaluated by ^{1}H NMR spectroscopic analysis in presence of TFA to break the hydrogen bonds after precipitation and drying of the polymers by integrating the peak at 3.50 ppm (Figure 3). The integrals of the signals **i** (3.5 ppm), **b** + **d** (5.5 ppm), and **c** (5.0 ppm) are used in eq 1 mentioned below to determine the grafting yield.

$$\mathrm{DF}\ (\%) = \frac{2 \times \frac{A_{3.5}}{2}}{A_{5.5} - \left(\frac{A_{5.0}}{2}\right)} \times \frac{11}{89} \times 100 \qquad (1)$$

To investigate the influence of the UPy content on the material properties, four different materials were synthesized with a varying thiol−UPy/alkene ratio of 5, 7, 10, and 15 mol % of thiols to vinyl side chains on the polymer. The grafting yield and corresponding conversions are displayed in Table 1. For consistency throughout the paper, the discussed UPy amounts will be relative to the vinyl side chains.

In the first experiment, 5% UPy was used in combination with a 10 mol % UV initiator, and a DF of 3.6% was achieved,

https://doi.org/10.1021/acs.macromol.1c01908
Macromolecules 2022, 55, 928−941

Scheme 2. Potential Intramolecular Cyclization Side Reactions in PB during the Thiol−Ene Reaction

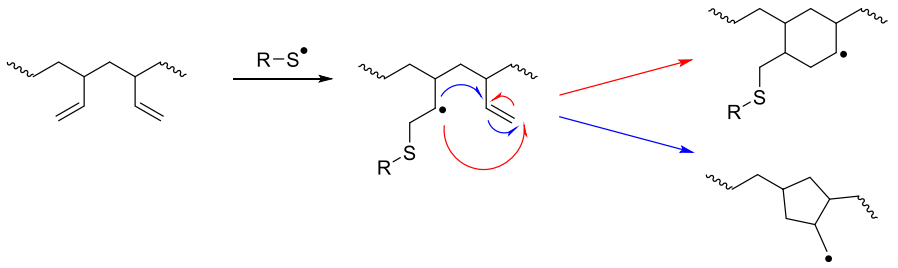

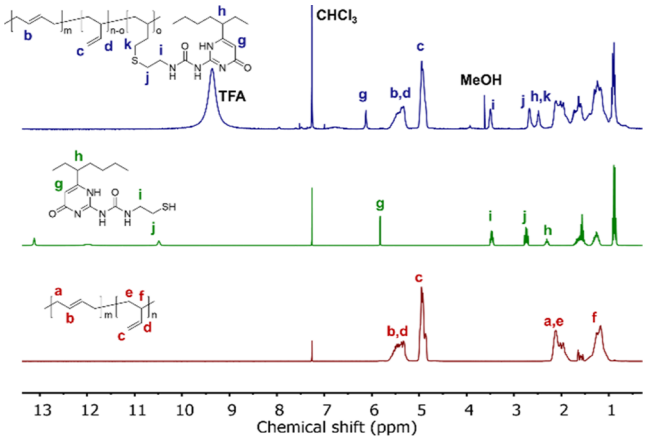

Figure 3. ^{1}H NMR spectra before and after the thiol−ene reaction of PB-U8.

Table 1. Results of the Thiol−Ene Reactions[a]

polymer	UPy (mol % to vinyl)	DF_{vinyl} (%)[b]	$DF_{polymer}$ (%)[c]	conversion (%)
PB-U4	5	3.6	3.2	72
PB-U6	7	6.3	5.6	89
PB-U8	10	8.2	7.3	82
PB-U13	15	13.1	11.6	87

[a]All reactions were executed at room temperature with an irradiation time of 2.5 h and a UV initiator content of 10 mol % per equivalent of thiol. [b]Degree of functionalization relative to the vinyl bonds of PB. [c]Degree of functionalization relative to the total amount of monomer units in the polymer.

corresponding with a 72% conversion of the thiols. The other polymers were synthesized in an identical way, resulting in UPy contents of 6.3, 8.2, and 13.1% relative to the vinyl bonds with conversions of 82% and higher. Interestingly, PB-U13 precipitated as a gel during the thiol−ene reaction. Next, the polymers were precipitated to remove the remaining reagents. Although PB-U6 to PB-U13 nicely precipitated in cold diethyl ether, the less cross-linked PB-U4 was still moderately soluble in diethyl ether and was therefore precipitated in cold methanol.

As unreacted UPy units could compromise the mechanical properties of the materials, diffusion-ordered spectroscopy (DOSY) was performed to ensure complete removal of the unreacted thiols (Figures 4 and S1−S3). A drop of trifluoroacetic acid (TFA) was added to ensure complete disruption of the hydrogen-bonding interactions in the NMR samples. The spectrum shows the same diffusion coefficient for the UPy and polymer signals, confirming the absence of free hydrogen-bonding moieties.

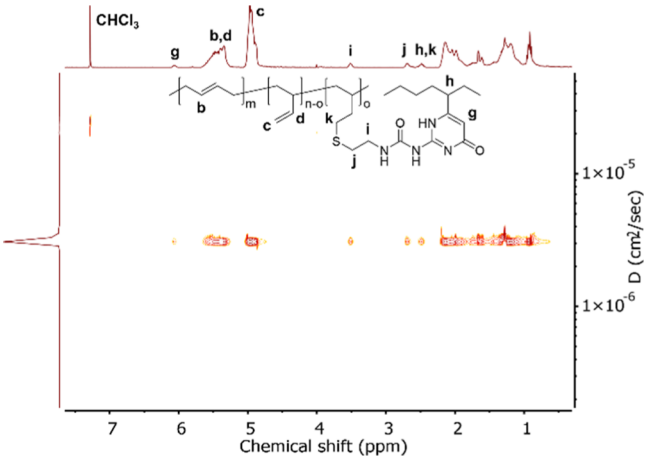

Figure 4. DOSY NMR spectrum of PB-U6 to demonstrate the absence of free UPy-SH in the purified polymer network.

The polymers were further characterized by SEC, and the results are summarized in Figure 5. Again, a drop of TFA was

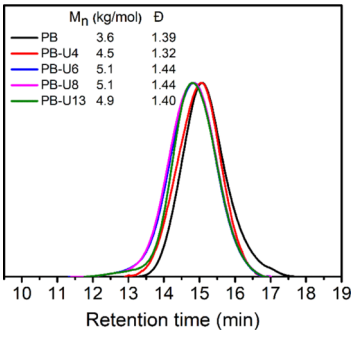

Figure 5. Overlay of normalized refractive index (RI) traces measured via SEC with THF as the eluent of the purified polymers with weight average molecular weight (M_w) and dispersity ($Đ$) relative to PMMA standards.

added to dissolve the polymers in THF. An increase in number average molecular weight (M_n) with increased UPy incorporation is observed up until PB-U6, stagnating at 8% UPy, while the value of PB-U13 drops a little below that of PB-U8. This apparent formation of a plateau value in molecular weight is potentially correlated with the hydrodynamic radius (R_h) of the polymer, which reaches a maximum at a certain critical UPy content, possibly due to intramolecular hydrogen bonding, leading to a lower R_h, once the TFA is separated from the polymer on the SEC column. This could be a possible explanation for the lower M_n of PB-U13 compared to the other polymers.

https://doi.org/10.1021/acs.macromol.1c01908
Macromolecules 2022, 55, 928−941

After purification and molecular characterization, the thermomechanical properties of the PB-UPys were analyzed. First, TGA was performed to investigate the thermal stability of the polymers (Figure S4). All polymers were stable up until 250 °C under a nitrogen atmosphere, after which an increased thermal degradation was observed with the increasing UPy content on the polymer. Next, DSC was performed to quantify the increase in glass transition temperature (T_g) with increasing cross-link density (Figure 6a). Within the evaluated

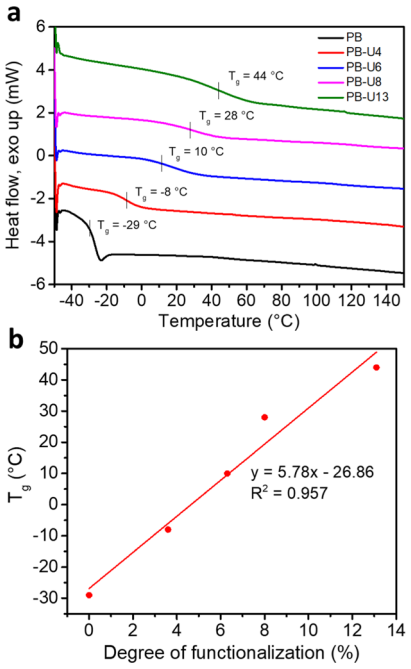

Figure 6. DSC results for the PB-UPy polymers. (a) DSC curves recorded during second heating of the samples and (b) correlation between the T_g and the UPy content of the polymer.

range of functionalization degrees, a fairly linear trend of the T_g as a function of the functionalization degree can be observed in Figure 6b. However, as both the chemical modification and physical cross-linking can influence the T_g and their individual contribution cannot be decoupled, these results should be interpreted with caution. Furthermore, visual inspection of thin films of the polymer materials prepared by compression molding showed clear transparent materials for PB-U4, PB-U6, and PB-U8, while some opaque spots were observed for PB-U13 indicating the occurrence of partial macroscopic phase separation (Figure S5), which might be rather minor as it could not be detected by DSC. Note that for PB end functionalized with methyl-UPy, consequently having a rather low DF, the phase separation was reported based on DSC. This indicates that the branched alkyl side chains indeed are capable of suppressing the phase separation of the UPy from PB.

The increasing T_g with the elevated UPy content can be partially explained by a decreased chain mobility with increased cross-link density, which increases the energy needed to break the physical cross-links and allows sufficient chain mobility, hence a higher T_g. Moreover, there seems to be a broadening of the glass transition with the increasing UPy content, which might be related to non-uniform distribution UPy cross-links among the polymer chains, due to the statistical nature of the post-polymerization modification step. Importantly, no melting peak was observed in the thermograms of all polymers, confirming the good compatibility of UPy with the polymer matrix as it is a good indication for the absence of significant phase-separated UPy clusters based on previous literature reports that could even confirm phase separation by DSC for PB that was chain end-functionalized methyl-UPy, as also discussed in the introduction.[36,52]

Further characterization was done by DMTA to investigate the thermomechanical properties of the supramolecular polymer networks. In Figure 7a, the evolution of the storage

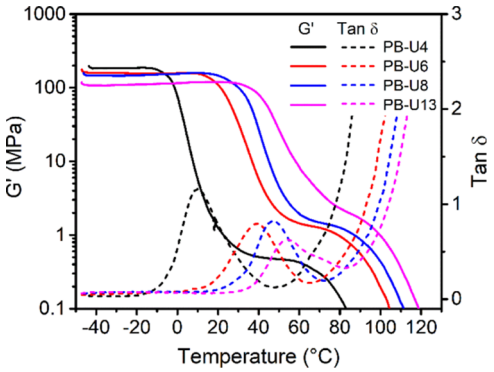

Figure 7. DMTA results of the polymer networks. The storage modulus (G') and tan δ are shown as a function of temperature.

modulus (G') with increasing temperature is displayed. The glassy region seems to extend with increasing cross-link density before the storage modulus, with values from 100 to 200 MPa, decays toward the rubber region. Furthermore, PB-U4 also displays a small rubbery plateau between 30 and 60 °C, which shifts to higher temperatures and higher-plateau moduli with increasing cross-link density and simultaneously becomes narrower, to completely disappear in PB-U13. The fact that the rubbery plateau is never extended over a large region can be ascribed to the absence of significant chain entanglements due to the low molecular weight of the polymer. Consequently, the polymers gain their physical strength almost completely from the UPy cross-links. Additionally, the flow points of the materials display the same trend as the rubbery plateau and increase with higher UPy incorporation. Indeed, the polymers with higher amounts of hydrogen-bonded cross-links may require more energy to dissociate a sufficiently large population of UPy dimers in order to allow material flow, which is expressed in the increase in the flow points with the increasing UPy content. However, the increase in the solid-to-liquid transition with the increasing UPy content might also be induced by the increase in T_g, as the glassy-to-rubbery and rubbery-to-liquid transitions cover similar temperature ranges and will be backed up by the similar calculated activation energies from the Arrhenius plot of the horizontal shift factors for PB-U6, PB-U8, and PB-U13 (Figure 11).

This can also be seen in Figure 7 where tan δ is plotted against temperature. For PB-U4, the peak maximum is the most pronounced, while it seems to decrease with increasing cross-link density. Additionally, the position of the maximum in tan δ also follows the same trend as observed in the DSC results for the T_g, that is, the maximum shifts to higher temperatures with a higher UPy content. The broader tan delta peak for PB-U13 is likely related to minor phase separation as indicated by the partial opaqueness of the sample (Figure S5).

https://doi.org/10.1021/acs.macromol.1c01908
Macromolecules 2022, 55, 928−941

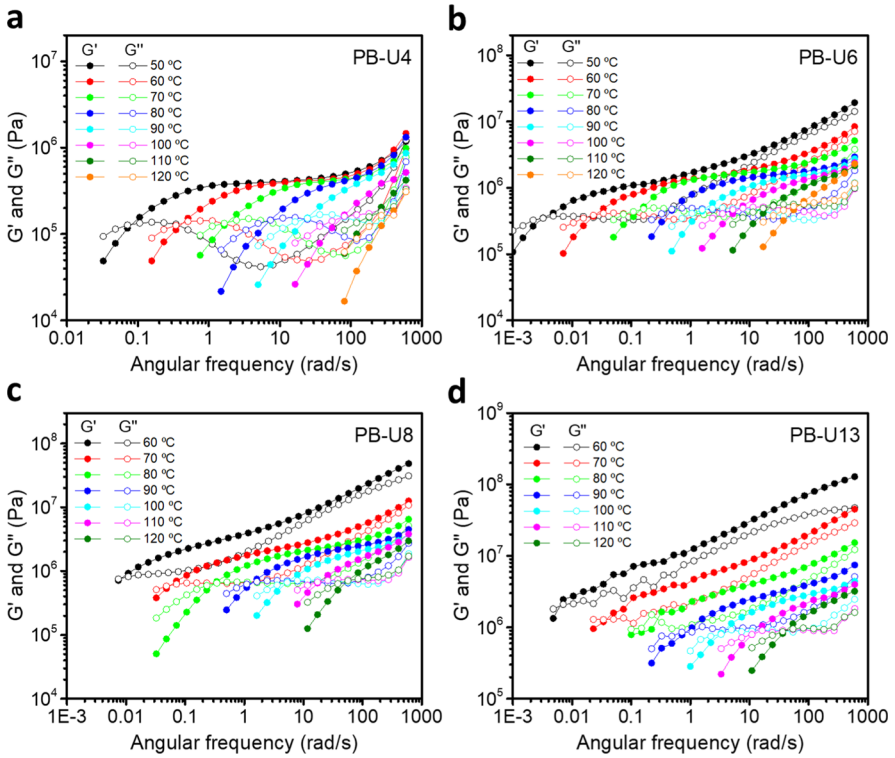

Figure 8. Frequency sweep data of the rheological characterization of the polymers at different temperatures.

In Figure S5, the polymer materials are presented after compression molding. By heating the samples, the hydrogen bonds become increasingly dynamic and ultimately completely dissociate, resulting in material flow, which was also observed in the DMTA data discussed above, and allowing the thermal processing of the PB-U materials. After pressing the viscous polymer melt into a mold, the material is allowed to cool down, decreasing the hydrogen-bond dynamics again, which restores the physical cross-links. Based on the DMTA results, PB-U4 was pressed at 80 °C, PB-U6 and PB-U8 at 100 °C, and PB-U13 at 120 °C. All films were nicely transparent, except for PB-U13 (not very clear in the picture because of the thin film). When a thicker film was pressed, opaque white regions appeared for PB-U13. These results indicate that the limit of UPy that can be homogeneously incorporated in the polymer matrix was exceeded in PB-U13, although no crystallization or melting was observed in the DSC measurements.

Linear Viscoelasticity. *Sticker Dynamics and Activation Energy.* The linear shear rheology of the PB-UPy systems was assessed by small amplitude oscillatory shear measurements. All the resulting frequency sweep data are displayed in Figure 8. It can be observed that the crossover points of the storage and loss modulus (G' and G'', respectively) shifted to higher frequencies with increasing temperature. Furthermore, when comparing the data at a specific temperature, it is observed that the relaxation time of the samples largely increases with increasing the cross-link density, consistent with the DMTA results. The PB-UPy polymers clearly show the formation of a transient network at temperatures up to 70 °C, as indicated by the formation of a plateau in G' despite the unentangled state of the building blocks. This rubbery plateau is much more well-defined for PB-U4 than for PB-U6 (Figure 8a,b, resp.), for which it only starts to appear below 70 °C. In the more densely cross-linked networks PB-U8 and PB-U13, a rubbery plateau can also be distinguished; however, the latter is less pronounced and is only visible at lower frequency.

In order to further analyze the sticker dynamics and to determine their activation energy, we followed the procedures described by Chen et al. and by the theory of Rubinstein and Semenov, to determine the temperature dependence of the renormalized lifetime of a supramolecular bond, τ_S.[53,54]

In Rubinstein–Semenov theory, in a reversible gel with strong associations, a sticker dissociates and reassociates several times with the same partner.[54] As a consequence, the stress related to the slow modes only starts to relax when one of the initially paired stickers has found a new partner. This process occurs at a timescale τ_S which is significantly longer than the bare sticker lifetime τ_S^*. Rubinstein and Semenov report that τ_S depends on the temperature via the relation

$$\tau_S \propto \tau_\nu \exp\left(\frac{E_a}{k_B T}\right) \tag{2}$$

where τ_ν is a local attempt time, E_a the activation energy of τ_S, and k_B the Boltzmann constant. As τ_ν depends on the chain mobility at a local level, it should have the same temperature dependence as the Rouse relaxation time of a Kuhn segment, τ_0, or equivalently, as the non-cross-linked PB sample.[53,55]

Thus, one notices that the dynamics of the systems are essentially controlled by two different timescales, τ_S and τ_0, which explains the thermo-rheological complexity of the samples. In order to distinguish both timescales, we use the time–temperature superposition principle (TTS) and follow the subsequent procedure described by Zhang at al.[56]

In Figure S6, the storage and the loss modulus, G' and G'', respectively, are first shifted by a factor a_T so that the response of the polymeric systems superimposes at high frequency. A vertical shift $b_T = \frac{\rho_{ref} T_{ref}}{\rho T} \approx \frac{T_{ref}}{T}$ has also been applied. (Note

https://doi.org/10.1021/acs.macromol.1c01908
Macromolecules 2022, 55, 928–941

that we assumed that the density changes over the used temperature range are negligible). As expected, these shifts lead to a failure in the superposition in the low-frequency part due to the stronger temperature dependence of the mechanism of the sticker dissociation. In a very similar way, the linear responses were shifted by factors a'_T and b_T so that the data coincide at low frequency. As observed in Figure S7, the curves cease to superimpose at high frequency, when the segmental motions start to contribute to the stress relaxation.

This procedure yields two sets of shift factors which allow to characterize the temperature dependence of the slow modes and the fast modes. As these shifts were collected at constant temperature, one needs to multiply them by a free volume correction factor a_{T_g} to compare them.[57] Details about the way we computed a_{T_g} can be found in Appendix A (see the Supporting Information).

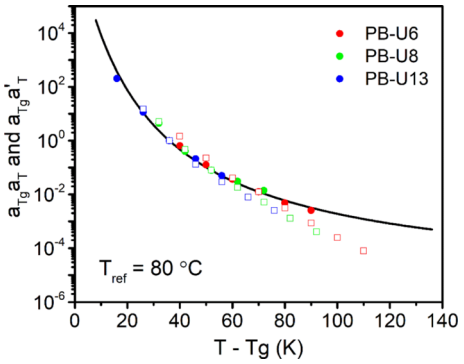

Figure 9. Corrected shift factors $a_T a_{T_g}$ (o) and $a'_T a_{T_g}$ (□) of PS systems as a function of $T-T_g$ at the reference temperature T_{ref} = 130 °C. The symbols are the experimental results, and the solid line is the predictions of the WLF equation.

As shown in Figure 9, after the correction is made, it is found that the shift factors $a_{T_g}a_T$ for the systems PB-U6, PB-U8, and PB-U13 are well described by the Williams–Landel–Ferry (WLF) equation[58]

$$\log_{10}\ a_{T_g}a_T = \frac{-c_1^0(T - T_{ref})}{c_2^0 + (T - T_{ref})} \tag{3}$$

with c_1^0 = 5.32 and c_2^0 = 61.36 K.

This allows to confirm that the high-frequency part is governed by the segmental motion of the polymeric chains.

On the other hand, the evolution of the factors $a_{T_g}a'_T$ with temperature can described by

$$a_{T_g}a'_T = a_T \exp\left(\frac{E_a}{R}\left(\frac{1}{T} - \frac{1}{T_{ref}}\right)\right) \tag{4}$$

Indeed, as shown in Figure 10, a linear dependence is found for the expression $\log(a'_T/a_T)$ as a function of $1000/T$. The corresponding values for E_a can therefore be obtained from a linear fitting, which leads to E_a ranging from 31.6 to 36.2 kJ/mol. These activation energies are comparable to E_a = 33–37 kJ/mol evaluated for PnBA-UPy by Zhang et al.[56]

It must be noted that in this procedure, we used the shifts a_T given by the WLF equation, which allows to widen the

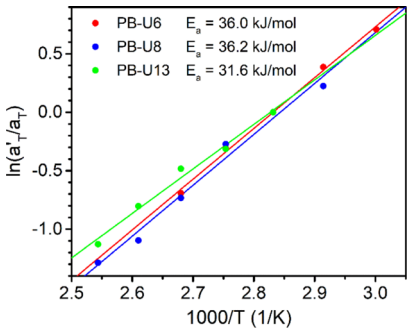

Figure 10. Extraction of the activation energy of PB-U6, PB-U8, and PB-U13 at T_{ref} = 80 °C.

temperature range in the regression. Note that the regression for PB-U6 was not performed beyond T = 100 °C as the WLF equation is invalid beyond $T/T_g > 1.3$.[59]

According to Rubinstein–Semenov theory, the activation energy of a reversible gel with strong associations can be expressed as

$$E_a = 1.5E_{binding} + E_{assoc} \tag{5}$$

where $E_{binding}$ is the binding energy, and E_{assoc} is the association energy, which corresponds to the activation energy of the bond formation.[54] Thus, E_{assoc} determines the time that two stickers must spend in the close vicinity of each other to form a bond, while $E_{binding}$ determines the average time in the associated state. By assuming that the renormalized lifetime τ_S is the relevant timescale for the dynamics at low frequencies, the inequality $E_{assoc} < E_{binding}/2$ should hold. As a result, the binding energy should be between $E_a/1.5$ and $E_a/2$. Within the experimental temperature range, $E_{binding}$ lies in an interval of $5.4k_BT$ and $8.2k_BT$. These values are in agreement with a very low density of open stickers as this is obtained if $\exp(E_{binding}/k_BT) \gg (M_s/M_K)^{1.5}$, with M_s being the average molar mass between two stickers and M_K the molar mass of a Kuhn segment.[60] According to Fetters et al., M_K is around 120 g/mol.[61]

Master Curve Construction. In order to model the data, it is convenient to summarize them into a single master curve corresponding to a specific temperature, T_{ref}. Despite the thermo-rheologically complex behavior of these systems, this can be achieved under specific conditions. In particular, it requires fixing a reference temperature T_{ref}, at which the storage and loss moduli data cover a wide frequency range that spans from the end of the relaxation of the fast modes to the beginning of the relaxation of the slow modes. Indeed, it is in this transition regime that thermo-rheological complexity is observed, the data following neither a WLF equation as in the high-frequency region nor an Arrhenius behavior, as in the low-frequency region. Therefore, it is important to ensure that the rubbery plateau is entirely described at $T = T_{ref}$. For the curves measured at $T < T_{ref}$, we apply shifts a_T and b_T so that they increases the frequency range in the part governed by the slow modes. In a very similar manner, the moduli obtained at $T > T_{ref}$ are shifted by a'_T and b_T to maximize the amount of information in the regime of the sticker dissociations. Finally, for the curves measured at $T < T_{ref}$ (resp. $T > T_{ref}$), we remove the data that correspond to the relaxation of the slow modes (resp. fast modes). The resulting master curves are shown in Figure 11a at T_{ref} = 80 °C and Figure 11b at T_{ref} = 60 °C (for

https://doi.org/10.1021/acs.macromol.1c01908
Macromolecules 2022, 55, 928–941

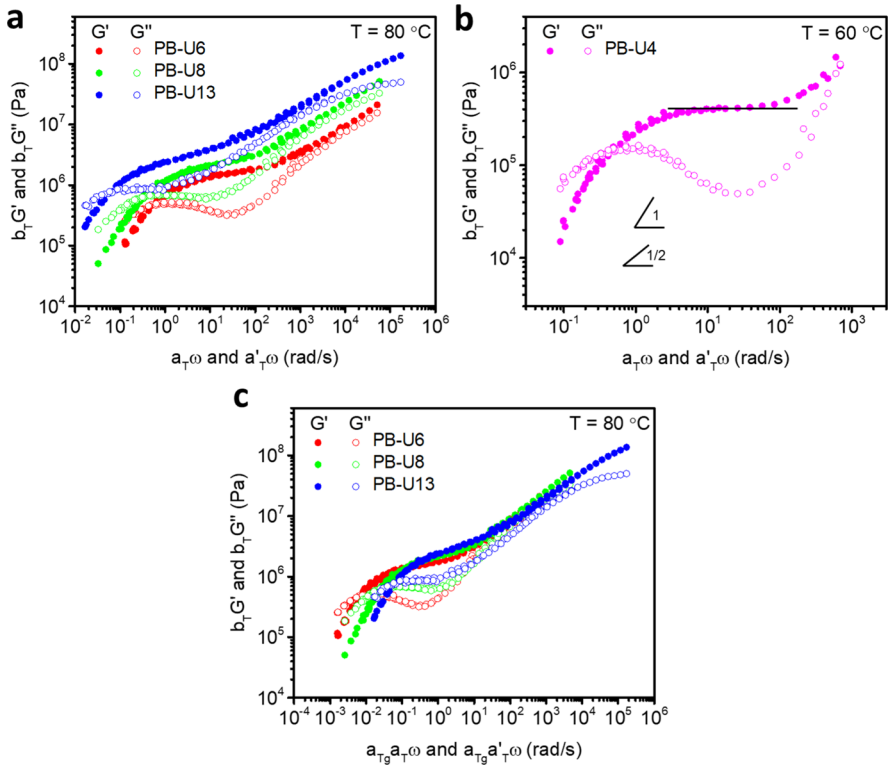

Figure 11. (a) Mastercurves of the systems PB-U13, PB-U8, and PB-U6 shown at T_{ref} = 80 °C. (b) Mastercurve of the systems PB-U4 shown at T_{ref} = 60 °C. The black line indicates the value of the plateau modulus $G_N^0 = \epsilon^{\frac{3\rho RT}{M_w}}$. (c) Mastercurves of the systems PB-U13, PB-U8, and PB-U6 obtained at T_{ref} = 80 °C and subsequently shifted by a factor a_{T_g}.

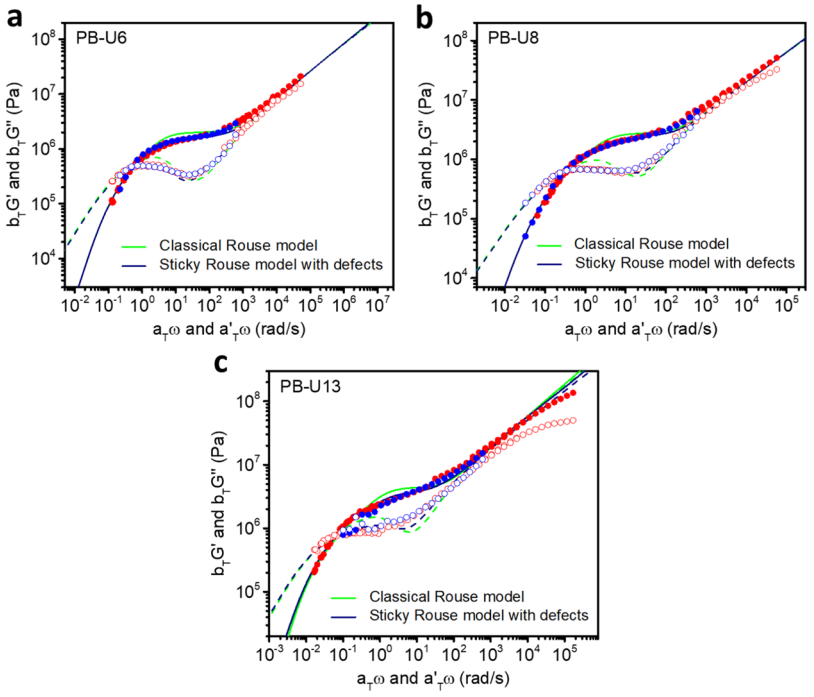

Figure 12. TTS master curves for (a) PB-U6, (b) PB-U8, and (c) PB-U13 at T_{ref} = 80 °C with the fitting results using the sticky Rouse model. Blue symbols correspond to the data measured at T_{ref} = 80 °C.

each sample, the experimental frequency window covered by the non-shifted data at T_{ref} is highlighted in Figure 12).

In associative polymers, the degree of gelation ϵ is defined in such a way that $\epsilon < 0$ is below the gel point, $\epsilon = 0$ is the gel point, and $\epsilon > 0$ is above. Also, when $0 < \epsilon < 1$, the chains have less than two intermolecular associations, and the system is a mixture of sol and gel, while for $\epsilon > 1$ (i.e., with more than two intermolecular associations), all the chains are involved in a

https://doi.org/10.1021/acs.macromol.1c01908
Macromolecules 2022, 55, 928−941

gel.[62] In the remainder of this section, we first study the relaxation of associative polymers with $\epsilon > 1$, which should correspond to the systems PB-U6, PB-U8, and PB-U13. Then, we will detail the case $0 < \epsilon < 1$ that applies to PB-U4 as seen later.

Figure 11a shows the effects of the increase in the mole fraction of the UPy groups on the rheological properties for the systems PB-U13, PB-U8, and PB-U6 of a very similar molar mass. In the high-frequency portion, the moduli scale with $\omega^{1/2}$ as the polymer chains relax only by the Rouse process. They do not superimpose as the increase in the T_g leads to larger monomeric friction coefficients. This regime continues until it is interrupted by the stickers.

Then, at intermediate frequencies, the systems display a rubbery plateau, which gradually increases in magnitude with the density of stickers. Indeed, associative bonds act as physical cross-links that prevent the chains to relax further. Increasing the amount of UPy makes the network more dense and leads to a higher plateau modulus as $G_N^0 \sim \frac{\rho RT}{M_s}$. Also, one can see a slight relaxation in the plateau regime that tends to increase with the UPy concentration. This effect is discussed in the next section.

Finally, at low frequency, one can observe that the longest relaxation time τ_{rel} tends to increase with the number of UPy groups in the polymeric chains. As these sticky chains are too short to be entangled, their dynamics should be well described by the sticky Rouse model.[53,55] In such a case, as further detailed in the next section, the terminal relaxation time, τ_{rel}, is given by the product $N_s^2\tau_S$, where N_S is the number of stickers along the chain backbone, and τ_S is the average lifetime of a sticker. Therefore, two effects that cause the increase in τ_{rel} can be distinguished:

- Increasing N_s augments the number of slow modes and therefore leads to a widening of the Rouse ramp.
- The increase in the T_g with the incorporation of the UPy groups slows down the segmental motion and therefore tends to make τ_s and τ_{rel} longer (see eq 4).

In order to have a meaningful comparison of the flow dynamics, one can remove the effects due to the different T_g by shifting horizontally the master curves by a factor a_{T_g}, as done in Figure 11c. As observed, the high-frequency regimes overlap, which means that the systems have similar segmental motion. However, a slight mismatch is obtained for the system PBU13. This discrepancy could possibly come from the experimental results obtained with the DSC, as an error of 4.1 °C in the $\Delta T_g = T_{g,PB\text{-}U13} - T_{g,PB\text{-}U8}$ is sufficient to explain it. Despite this, one can see that under iso-T_g conditions, τ_{rel} tends to decrease with the grafting of the UPy groups. In the literature, a similar result has already been obtained by Cui et al. for the copolymers UPyPEHA composed of ethylhexyl acrylate (EHA) and 2-[3-(6-methyl-4-oxo-1,4-dihydropyrimidin-2-yl)ureido]-ethyl acrylate (UPyEA).[55] Indeed, they report that the ratio τ_s/τ_0 tends to decrease with the addition of the UPyEA. This trend is in contradiction with the scaling laws obtained by Rubinstein and Semenov, according to which, a larger density of stickers increases the number of returns of a pair of stickers N_{Ret}, as it depends on the ratio of the probability that two stickers of a pair come close to each other P_r to the equilibrium fraction of open stickers ϕ_{open}. Thus, adding associative groups should lead to a longer τ_S as P_r increases faster than ϕ_{open}^{-1} decreases.[54]

The master curve of the system PB-U4 is depicted in Figure 11b. At high frequency, the moduli scale linearly with the frequency. In this regime, the stress relaxation is mainly due to the diffusion of the clusters formed by mean-field percolation. Then, at lower frequencies, the systems show a well-defined plateau. This one is slightly lower than $\rho RT/M_w$, which suggests that the system is indeed a mixture of sol and gel.[63] From the value of the plateau $G_N^0 \sim \rho RT/M_w\epsilon^3$, one obtains a degree of gelation $\epsilon = 0.95$. Finally, at low frequency, one can see that $G' \propto \omega^2$ and $G'' \propto \omega$, as predicted by the Maxwell model. From these scaling laws, one can estimate the relaxation time via eq 6.[63]

$$\tau = \lim_{\omega \to 0} \frac{G'(\omega)}{\omega G''(\omega)} \approx 3.02 \text{ s} \tag{6}$$

This leads to a value for τ_S of 3.17 s as $\tau \approx \epsilon\tau_S$.

Modeling the Linear Viscoelastic Properties. Relaxation Modulus of Free Unentangled Chains. Free unentangled chains relax through the Rouse process. The relaxation is described by N relaxation modes, each one characterized by its own characteristic time. The pth relaxation time, with p ranging from 1 to N, corresponds to the average duration taken by chain subsections containing N/p Kuhn segments to recover from the perturbation induced by the strain. As all the modes are orthogonal, they can be summed, and the Rouse relaxation modulus can be written as

$$G(t) = \sum_i \frac{\rho w_i RT}{M_{w,i}} \sum_{p=1}^{N_i} \exp\left(-\frac{tp^2}{\tau_0 N_i^2}\right) \tag{7}$$

where ρ is the mass density, T is the absolute temperature, R is the ideal gas constant, N is the number of Kuhn segments per chain, τ_0 is the relaxation time of a Kuhn segment, and w is the weight fraction.[64,65] The first summation term in eq 7 takes into account polydispersity in molar mass.

Relaxation Modulus of Associative Polymers. Relaxation modulus of the reversible network regime ($\epsilon > 1$). Relaxation modes involving subchains smaller than the average length between two associative bonds M_s, should not be influenced by the connectivity of the chain. As a result, these modes called "fast modes" can be described by a Rouse process. In contrast, the modes corresponding to the collective motion of segments larger than M_s undergo an extra drag due to the associative bonds. In the sticky Rouse model, these "slow" modes are uniformly delayed and described by a low-order Rouse process.[66] On this basis, Chen et al. expressed the relaxation modulus of a reversible network as

$$G(t) = \sum_i \frac{\rho w_i RT}{M_{w,i}} \left(\sum_{p=N_{s,i}+1}^{N_i} \exp\left(-\frac{tp^2}{\tau_0 N_i^2}\right) + \sum_{p=1}^{N_{s,i}} \exp\left(-\frac{tp^2}{\tau_S N_{S,i}^2}\right) \right) \tag{8}$$

where $N_{s,i} = M_{w,i}/M_s$ is the number of stickers per chain, and τ_S is the association lifetime.[53]

The inequality $\tau_S N_S^2 \geq \tau_0 N^2$ is needed to obtain the delaying effect caused by the associations. Note that in the expression of the slow modes, it is assumed that the friction of the backbone is negligible compared to that of the associative bonds.

https://doi.org/10.1021/acs.macromol.1c01908
Macromolecules 2022, 55, 928−941

One can generally observe a good qualitative match of the sticky Rouse model (eq 8) with experimental data. However, significant discrepancy with the data still persists, especially in the rubbery plateau regime. That is why few modifications of the model have been proposed to improve the fitting. Among them, one can distinguish the two following shortcomings of the model.

Equation 8 neglects the contribution to the response from dangling ends. As done by Cui et al., one can correct this by decomposing the fast modes into two contributions coming from the dangling ends and the trapped segments[55]

$$G_{\text{fast}}(t) = \sum_i \frac{\rho w_i RT}{M_{\text{w},i}} (G_{\text{ends}}(t) + G_{\text{trapped}}) \tag{9}$$

where $G_{\text{ends}}(t)$ and $G_{\text{trapped}}(t)$ are given by

$$G_{\text{ends}}(t) = \phi_{\text{ends}} \sum_{p=N_{s,i}+1, p \text{ odd}}^{N_i} \exp\left(-\frac{tp^2}{4\tau_0 N_i^2}\right) \tag{10}$$

$$G_{\text{trapped}}(t) = \phi_{\text{trapped}} \sum_{p=N_{s,i}+1}^{N_i} \exp\left(-\frac{tp^2}{\tau_0 N_i^2}\right) \tag{11}$$

Here, ϕ_{end} and ϕ_{trapped} are respectively the weight fraction of the chains ends and that of the trapped segments.

In addition to the polydispersity in molecular weight, one needs to take into account a dispersity in the distribution of the number of stickers per chain due to the statistical nature of the modification process.[67,68] As each of the N_i Kuhn segments has a probability $p_i = 1/N_{s,i}$ to be associative, the number of stickers per chain of molar mass $M_{w,i}$ follows a Poisson distribution $\text{Pois}(N_i p_i)$ as it approximates the binomial distribution very well, as demonstrated by the Poisson limit theorem.

$$p_{s,i}(X = k) = \frac{\lambda_i^k \, e^{-\lambda_i}}{k!} \text{ with } \lambda_i = \frac{N_i}{N_{s,i}} \tag{12}$$

Relaxation modulus of the mixture of sol and gel ($0 < \epsilon < 1$). When there are less than two intermolecular associations, chains start to assemble into distinct clusters, and the mechanism of relaxation changes. In this subsection, we consider systems with slightly less than two intermolecular associations so that chains strongly overlap and that the system stays a mixture of sol and gel. As a result, the amount of intramolecular associations should stay limited, and mean-field percolation statistics should be valid.[62]

At short time, the dynamics are controlled by the Rouse process as it involves the motion of portions of the chains that are smaller than M_S. Then, the stress relaxation is essentially controlled by the diffusion of the clusters as a whole. In this regime, the G' and G'' scale linearly with the pulsation ω. These ones relax in a timescale $\tau_{\text{rel}}(M_{\text{cluster}}) \sim \frac{\tau_R}{\epsilon^3}$. After this, the gel starts to manifest as a plateau $G_N^0 \sim \frac{\rho RT}{M_w}\epsilon^3$. Finally, at a timescale $\tau_{\text{max}} \sim \tau_S \epsilon$, the network breaks, which allows the system to relax completely.[54] A summary of the scaling laws of the storage modulus for the case $\epsilon > 1$ and $0 < \epsilon < 1$ can be found in Figure S8.

Comparison with the Experimental Data. Figure 12 shows the prediction of the sticky Rouse model with the two modifications described in eqs 9−12. The number of stickers has been fixed consistently with the sample composition. The results were converted to the frequency domain using Fourier transform. The $Đ$ has been incorporated into the sticky Rouse model via a log-normal distribution (see Appendix B in the Supporting Information).

At intermediate frequencies, it is observed that the model does not allow to correctly describe the experimental data, despite the fact that both the influence of dangling ends and the polydispersity of the sticker position have been accounted for. The main cause of this is that the data show significant relaxation in the rubbery plateau region, that the model does not predict since it is assumed that in this regime, the sample relaxation is frozen as long as the time is shorter than the sticker lifetime, τ_s. As the missing relaxation occurs close to the local minima of G'', this discrepancy could be due to the Rouse modes of motional units larger than the trapped segments, coming from the presence of defects in the network, such as elastically ineffective pending loops resulting, for example, from dimerization of two UPy units on the same polymer chain, which tends to increase the length of the elastically effective strands. For example, as depicted in Scheme 3, the strands that contain one such loop have an effective length of $2M_s$, that is twice the size of the trapped segments in the ideal network, while the pending loop acts as an extra friction point for the motions of the strands. If we limit ourselves to this case and thus, neglect the strands of length higher than $2M_s$, the relaxation modulus can be expressed as

Scheme 3. Elastically Ineffective Loops in the Structure of the Network Caused by Dimerization of Two UPy Units on the Same Polymer Chain

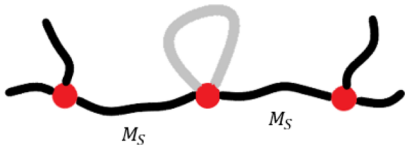

$$G(t) = \sum_i \frac{\rho w_i RT}{M_{\text{w},i}} \left(\sum_{p=1}^{N_{s,i}/2} \exp\left(-\frac{tp^2}{\tau_s N_{s,i}^2}\right) + (1 - \phi_{\text{loop}}) \sum_{p=(N_s/2)+1}^{N_{s,i}} \exp\left(-\frac{tp^2}{\tau_s N_{s,i}^2}\right) + \phi_{\text{loop}} \sum_{p=(N_{s,i}/2)+1}^{N_{s,i}} \exp\left(-\frac{tp^2}{\tau_f N_i^2}\right) \right) + G_{\text{fast}}(t) \tag{13}$$

where ϕ_{loop} is the weight fraction of the strands of length $2M_s$. Also, instead of τ_0, a characteristic time τ_f must be used in the expression of the Rouse modes of subchains larger than M_s to account for the friction brought by the pending loops. This time can be evaluated using an approach very similar to the one that was used by Papagiannopoulos et al. to estimate the relaxation time of unentangled comb polyelectrolytes.[69]

The characteristic time of a Kuhn segment, that is directly connected to a loop of length M_s, is defined by the relaxation time of that loop, which is $\tau_R \approx (M_s/M_K)^2 \tau_0$. Also, the Kuhn segments with no loops attached will relax in a time equal to τ_0. Based on this, one can compute τ_f by taking the average over all the Kuhn segments.

https://doi.org/10.1021/acs.macromol.1c01908
Macromolecules 2022, 55, 928−941

$$\tau_f = \frac{2\left(\frac{M_s}{M_K}\right) - 1}{2\left(\frac{M_s}{M_K}\right)}\tau_0 + \frac{1}{2\left(\frac{M_s}{M_K}\right)}\left(\frac{M_s}{M_K}\right)^2\tau_0 \approx \tau_0\left(1 + \frac{M_s}{2M_K}\right) \quad (14)$$

As seen in Figure 12, incorporating these loops improves the theoretical description of the viscoelastic curves. In spite of it, discrepancies still persist. As shown in Figures S9, S10, and S11 in Appendix A, one can see a mismatch of the theoretical prediction of G'' with the experimental results at low temperatures. Indeed, the model does not predict the shift of the local minima of G'' toward the low frequency and the decreasing ratio G''/G' with temperature at this level of the curve. This could be linked to a change of the structure of the network, which could bring further Rouse modes. Obviously, much more rigorous treatments of these topological defects, such as done by Panyukov,[70] could potentially refine the fitting.

The fitting parameters are summarized in Table 2. As discussed in the preceding section, a close inspection of Table 2 shows that the ratio τ_S/τ_0 tends to decrease with the amount of UPy.

Table 2. Fitting Parameters of the Sticky Rouse Model

τ_0^a [s]	τ_0 [s]	τ_s [s]	M_s [g/mol]	ϕ_{loop}
PB-U6	2×10^{-5}	0.4	1150	0.25
PB-U8	1.38×10^{-4}	0.6	850	0.35
PB-U13	1×10^{-3}	4	600	0.5

CONCLUSIONS

In summary, we have demonstrated the successful synthesis of a thiol-functional UPy unit with a branched alkyl side chain and its facile coupling onto 1,2-PB via thiol−ene chemistry. The incorporation of UPy and absence of free UPy in the obtained PB-UPys were confirmed by DOSY NMR spectroscopy. The TGA thermograms displayed the good thermostability of the networks, DSC showed an increasing T_g with the elevating UPy content in the networks, and the lack of a melting peak also indicated the absence of significant UPy phase separation, albeit minor microscopic phase separation was observed for PB-U13 as indicated by the appearance of opaque spots in injection-molded thin films. The complete absence of phase separation for PB-U4, PB-U6, and PB-U8 has to be interpreted with caution as additional characterization with microscopy and/or scattering experiments is needed to be conclusive that there is no phase separation at all. Nonetheless, previously reported PB end functionalized with methyl-UPy revealed phase separation in DSC, indicating that the here employed UPy with a branched aliphatic side chain can indeed suppress phase separation in a PB matrix. DMTA visualized the improved flow resistance with increased cross-link density, accompanied with the loss of dynamic properties. Linear viscoelasticity also showed the formation of the network with a plateau modulus and a terminal relaxation time which increase in magnitude with the density of stickers. The storage and the loss moduli were fitted with the sticky Rouse model. We found that the model does not allow to correctly describe the experimental data at intermediate frequency. This deviation was attributed to the presence of topological defects in the systems.

ASSOCIATED CONTENT

Supporting Information

The Supporting Information is available free of charge at https://pubs.acs.org/doi/10.1021/acs.macromol.1c01908.

Additional experimental and modeling data (PDF)

AUTHOR INFORMATION

Corresponding Author

Richard Hoogenboom − *Supramolecular Chemistry Group, Centre of Macromolecular Chemistry (CMaC), Department of Organic and Macromolecular Chemistry, Ghent University, B-9000 Ghent, Belgium;* orcid.org/0000-0001-7398-2058; Email: richard.hoogenboom@UGent.be

Authors

Jente Verjans − *Supramolecular Chemistry Group, Centre of Macromolecular Chemistry (CMaC), Department of Organic and Macromolecular Chemistry, Ghent University, B-9000 Ghent, Belgium*

Alexis André − *Bio- and Soft Matter, Institute of Condensed Matter and Nanosciences, Université catholique de Louvain, B-1348 Louvain-la-Neuve, Belgium; Department of Chemical Engineering, Katholieke Universiteit Leuven, B-3001 Leuven, Belgium*

Evelyne Van Ruymbeke − *Bio- and Soft Matter, Institute of Condensed Matter and Nanosciences, Université catholique de Louvain, B-1348 Louvain-la-Neuve, Belgium;* orcid.org/0000-0001-7633-0194

Complete contact information is available at: https://pubs.acs.org/10.1021/acs.macromol.1c01908

Notes

The authors declare no competing financial interest.

ACKNOWLEDGMENTS

J.V. and R.H. thank Ghent University for funding this work through the concerted research actions scheme. This work was partially funded by DSM Materials Science Center (AA) and by the French Community of Belgium through ARC project no 16/21-076 (A.A. and E.V.R.). E.V.R. is the Research Associate of the FRS-FNRS.

REFERENCES

(1) Dai, S.; Ravi, P.; Tam, K. C. PH-Responsive Polymers: Synthesis, Properties and Applications. *Soft Matter* **2008**, *4*, 435.

(2) Mane, S. R.; Sathyan, A.; Shunmugam, R. Biomedical Applications of PH-Responsive Amphiphilic Polymer Nanoassemblies. *ACS Appl. Nano Mater.* **2020**, *3*, 2104−2117.

(3) Bertrand, O.; Gohy, J.-F. Photo-Responsive Polymers: Synthesis and Applications. *Polym. Chem.* **2017**, *8*, 52−73.

(4) Stoychev, G.; Kirillova, A.; Ionov, L. Light-Responsive Shape-Changing Polymers. *Adv. Opt. Mater.* **2019**, *7*, 1900067.

(5) Hoogenboom, R. Temperature-Responsive Polymers: Properties, Synthesis and Applications. *Smart Polymers and their Applications*; Elsevier, 2014, pp 15−44.

(6) de la Rosa, V. R.; Woisel, P.; Hoogenboom, R. Supramolecular Control over Thermoresponsive Polymers. *Mater. Today* **2016**, *19*, 44−55.

(7) Jain, A.; George, S. J. New Directions in Supramolecular Electronics. *Mater. Today* **2015**, *18*, 206−214.

(8) Voorhaar, L.; Hoogenboom, R. Supramolecular Polymer Networks: Hydrogels and Bulk Materials. *Chem. Soc. Rev.* **2016**, *45*, 4013−4031.

(9) Dong, R.; Pang, Y.; Su, Y.; Zhu, X. Supramolecular Hydrogels: Synthesis, Properties and Their Biomedical Applications. *Biomater. Sci.* **2015**, *3*, 937−954.
(10) Obert, E.; Bellot, M.; Bouteiller, L.; Andrioletti, F.; Lehen-Ferrenbach, C.; Boué, F. Both Water- and Organo-Soluble Supramolecular Polymer Stabilized by Hydrogen-Bonding and Hydrophobic Interactions. *J. Am. Chem. Soc.* **2007**, *129*, 15601−15605.
(11) Klymenko, A.; Nicolai, T.; Benyahia, L.; Chassenieux, C.; Colombani, O.; Nicol, E. Multiresponsive Hydrogels Formed by Interpenetrated Self-Assembled Polymer Networks. *Macromolecules* **2014**, *47*, 8386−8393.
(12) Burattini, S.; Greenland, B. W.; Chappell, D.; Colquhoun, H. M.; Hayes, W. Healable Polymeric Materials: A Tutorial Review. *Chem. Soc. Rev.* **2010**, *39*, 1973−1985.
(13) Lin, Q.; Guan, X.-W.; Song, S.-S.; Fan, H.; Yao, H.; Zhang, Y.-M.; Wei, T.-B. A novel supramolecular polymer π-gel based on bis-naphthalimide functionalized-pillar[5]arene for fluorescence detection and separation of aromatic acid isomers. *Polym. Chem.* **2019**, *10*, 253−259.
(14) Appel, E. A.; Biedermann, F.; Rauwald, U.; Jones, S. T.; Zayed, J. M.; Scherman, O. A. Supramolecular Cross-Linked Networks via Host−Guest Complexation with Cucurbit[8]uril. *J. Am. Chem. Soc.* **2010**, *132*, 14251−14260.
(15) Del Valle, E. M. M. Cyclodextrins and Their Uses: A Review. *Process Biochem.* **2004**, *39*, 1033−1046.
(16) Rodell, C. B.; Mealy, J. E.; Burdick, J. A. Supramolecular Guest-Host Interactions for the Preparation of Biomedical Materials. *Bioconjugate Chem.* **2015**, *26*, 2279−2289.
(17) Burnworth, M.; Tang, L.; Kumpfer, J. R.; Duncan, A. J.; Beyer, F. L.; Fiore, G. L.; Rowan, S. J.; Weder, C. Optically Healable Supramolecular Polymers. *Nature* **2011**, *472*, 334−337.
(18) Li, C. H.; Zuo, J. L. Self-Healing Polymers Based on Coordination Bonds. *Adv. Mater.* **2019**, *32*, 1903762.
(19) Lai, J.-C.; Jia, X.-Y.; Wang, D.-P.; Deng, Y.-B.; Zheng, P.; Li, C.-H.; Zuo, J.-L.; Bao, Z. Thermodynamically Stable Whilst Kinetically Labile Coordination Bonds Lead to Strong and Tough Self-Healing Polymers. *Nat. Commun.* **2019**, *10*, 1164.
(20) Wathier, M.; Grinstaff, M. W. Synthesis and Properties of Supramolecular Ionic Networks. *J. Am. Chem. Soc.* **2008**, *130*, 9648−9649.
(21) Aboudzadeh, A.; Fernandez, M.; Muñoz, M. E.; Santamaría, A.; Mecerreyes, D. Ionic Supramolecular Networks Fully Based on Chemicals Coming from Renewable Sources. *Macromol. Rapid Commun.* **2014**, *35*, 460−465.
(22) Voorhaar, L.; Diaz, M. M.; Leroux, F.; Rogers, S.; Abakumov, A. M.; Van Tendeloo, G.; Van Assche, G.; Van Mele, B.; Hoogenboom, R. Supramolecular Thermoplastics and Thermoplastic Elastomer Materials with Self-Healing Ability Based on Oligomeric Charged Triblock Copolymers. *NPG Asia Mater.* **2017**, *9*, No. e385.
(23) Lange, R. F. M.; Van Gurp, M.; Meijer, E. W. Hydrogen-Bonded Supramolecular Polymer Networks. *J. Polym. Sci., Part A: Polym. Chem.* **1999**, *37*, 3657−3670.
(24) ten Brinke, G.; Ruokolainen, J.; Ikkala, O. Supramolecular Materials Based On Hydrogen-Bonded Polymers. *Hydrogen Bonded Polymers*; Advances in Polymer Science; Springer, 2007; Vol. *207*, pp 113−177.
(25) Cordier, P.; Tournilhac, F.; Soulié-Ziakovic, C.; Leibler, L. Self-Healing and Thermoreversible Rubber from Supramolecular Assembly. *Nature* **2008**, *451*, 977−980.
(26) Agnaou, R.; Capelot, M.; Tencé-Girault, S.; Tournilhac, F.; Leibler, L. Supramolecular Thermoplastic with 0.5 Pa·s Melt Viscosity. *J. Am. Chem. Soc.* **2014**, *136*, 11268−11271.
(27) Sijbesma, R. P.; Beijer, F. H.; Brunsveld, L.; Folmer, B. J. B.; Hirschberg, J. H. K. K.; Lange, R. F. M.; Lowe, J. K. L.; Meijer, E. W. Reversible Polymers Formed from Self-Complementary Monomers Using Quadruple Hydrogen Bonding. *Science* **1997**, *278*, 1601−1604.
(28) Folmer, B. J. B.; Sijbesma, R. P.; Versteegen, R. M.; van der Rijt, J. A. J.; Meijer, E. W. Supramolecular Polymer Materials: Chain Extension of Telechelic Polymers Using a Reactive Hydrogen-Bonding Synthon. *Adv. Mater.* **2000**, *12*, 874−878.
(29) Dankers, P. Y. W.; Harmsen, M. C.; Brouwer, L. A.; Van Luyn, M. J. A.; Meijer, E. W. A Modular and Supramolecular Approach to Bioactive Scaffolds for Tissue Engineering. *Nat. Mater.* **2005**, *4*, 568−574.
(30) van Gemert, G. M. L.; Peeters, J. W.; Söntjens, S. H. M.; Janssen, H. M.; Bosman, A. W. Self-Healing Supramolecular Polymers In Action. *Macromol. Chem. Phys.* **2012**, *213*, 234−242.
(31) Mather, B. D.; Elkins, C. L.; Beyer, F. L.; Long, T. E. Morphological Analysis of Telechelic Ureidopyrimidone Functional Hydrogen Bonding Linear and Star-Shaped Poly(Ethylene-Co-Propylene)S. *Macromol. Rapid Commun.* **2007**, *28*, 1601−1606.
(32) Botterhuis, N. E.; van Beek, D. J. M.; van Gemert, G. M. L.; Bosman, A. W.; Sijbesma, R. P. Self-Assembly and Morphology of Polydimethylsiloxane Supramolecular Thermoplastic Elastomers. *J. Polym. Sci., Part A: Polym. Chem.* **2008**, *46*, 3877−3885.
(33) Feldman, K. E.; Kade, M. J.; Meijer, E. W.; Hawker, C. J.; Kramer, E. J. Model Transient Networks from Strongly Hydrogen-Bonded Polymers. *Macromolecules* **2009**, *42*, 9072−9081.
(34) Appel, W. P. J.; Portale, G.; Wisse, E.; Dankers, P. Y. W.; Meijer, E. W. Aggregation of Ureido-Pyrimidinone Supramolecular Thermoplastic Elastomers into Nanofibers: A Kinetic Analysis. *Macromolecules* **2011**, *44*, 6776−6784.
(35) Monemian, S.; Jang, K.-S.; Ghassemi, H.; Korley, L. T. J. Probing the Interplay of Ultraviolet Cross-Linking and Noncovalent Interactions in Supramolecular Elastomers. *Macromolecules* **2014**, *47*, 5633−5642.
(36) Kan, L.; Zhang, P.; Jiang, H.; Zhang, S.; Liu, Z.; Zhang, X.; Ma, N.; Qiu, D.; Wei, H. Microphase Separation of a Quadruple Hydrogen Bonding Supramolecular Polymer: Effect of the Steric Hindrance of the Ureido-Pyrimidone on Their Viscoelasticity. *RSC Adv.* **2019**, *9*, 8905−8911.
(37) Jangizehi, A.; Ahmadi, M.; Seiffert, S. Emergence, Evidence, and Effect of Junction Clustering in Supramolecular Polymer Materials. *Mater. Adv.* **2021**, *2*, 1425−1453.
(38) Keizer, H. M.; Sijbesma, R. P.; Meijer, E. W. The Convenient Synthesis of Hydrogen-Bonded Ureidopyrimidinones. *Eur. J. Org. Chem.* **2004**, *2004*, 2553−2555.
(39) Hoyle, C. E.; Bowman, C. N. Thiol-Ene Click Chemistry. *Angew. Chem., Int. Ed.* **2010**, *49*, 1540−1573.
(40) Clay, R. J.; Collom, T. A.; Karrick, G. L.; Wemple, J. A Safe, Economical Method for the Preparation of β-Oxo Esters. *Synthesis* **1993**, *1993*, 290−292.
(41) Beijer, F. H.; Sijbesma, R. P.; Kooijman, H.; Spek, A. L.; Meijer, E. W. Strong Dimerization of Ureidopyrimidones via Quadruple Hydrogen Bonding. *J. Am. Chem. Soc.* **1998**, *120*, 6761−6769.
(42) Peng, H.-Q.; Sun, C.-L.; Xu, J.-F.; Niu, L.-Y.; Chen, Y.-Z.; Wu, L.-Z.; Tung, C.-H.; Yang, Q.-Z. Convenient Synthesis of Functionalized Bis-Ureidopyrimidinones Based on Thiol-Yne Reaction. *Chem.—Eur. J.* **2014**, *20*, 11699−11702.
(43) Salle, R.; Pham, Q.-T. Polymérisation anionique des dienes. VI. Microstructure des polybutadiène et polyisoprène par résonance magnétique protonique à 250 MHz et mécanismes de propagation. *J. Polym. Sci., Polym. Chem. Ed.* **1977**, *15*, 1799−1810.
(44) Ameduri, B.; Boutevin, B.; Nouiri, M. Synthesis and Properties of Fluorinated Telechelic Macromolecular Diols Prepared by Radical Grafting of Fluorinated Thiols onto Hydroxyl-Terminated Polybutadienes. *J. Polym. Sci., Part A: Polym. Chem.* **1993**, *31*, 2069−2080.
(45) Justynska, J.; Hordyjewicz, Z.; Schlaad, H. Toward a Toolbox of Functional Block Copolymers via Free-Radical Addition of Mercaptans. *Polymer* **2005**, *46*, 12057−12064.
(46) ten Brummelhuis, N.; Diehl, C.; Schlaad, H.; Brummelhuis, N. T.; Diehl, C.; Schlaad, H. Thiol−Ene Modification of 1,2-Polybutadiene Using UV Light or Sunlight. *Macromolecules* **2008**, *41*, 9946−9947.
(47) Lotti, L.; Coiai, S.; Ciardelli, F.; Galimberti, M.; Passaglia, E. Thiol-Ene Radical Addition of L -Cysteine Derivatives to Low

https://doi.org/10.1021/acs.macromol.1c01908
Macromolecules 2022, 55, 928−941

Molecular Weight Polybutadiene. *Macromol. Chem. Phys.* **2009**, *210*, 1471−1483.
(48) David, R. L. A.; Kornfield, J. A. Facile, Efficient Routes to Diverse Protected Thiols and to Their Deprotection and Addition to Create Functional Polymers by Thiol−Ene Coupling. *Macromolecules* **2008**, *41*, 1151−1161.
(49) Serniuk, G. E.; Banes, F. W.; Swaney, M. W. Study of the Reaction of Buna Rubbers with Aliphatic Mercaptans1. *J. Am. Chem. Soc.* **1948**, *70*, 1804−1808.
(50) Oswald, A. A.; Griesbaum, K.; Thaler, W. A.; Hudson, B. E. Organic Sulfur Compounds. VIII. Addition of Thiols to Conjugated Diolefins. *J. Am. Chem. Soc.* **1962**, *84*, 3897−3904.
(51) Ameduri, B.; Berrada, K.; Boutevin, B.; Bowden, R. D. Synthesis of a Telechelic Monodispersed Mercapto-Alcohol. *Polym. Bull.* **1993**, *31*, 1−7.
(52) Bobade, S. L.; Malmgren, T.; Baskaran, D. Micellar-Cluster Association of Ureidopyrimidone Functionalized Monochelic Polybutadiene. *Polym. Chem.* **2014**, *5*, 910−920.
(53) Chen, Q.; Tudryn, G. J.; Colby, R. H. Ionomer Dynamics and the Sticky Rouse Model. *J. Rheol.* **2013**, *57*, 1441−1462.
(54) Rubinstein, M.; Semenov, A. N. Thermoreversible Gelation in Solutions of Associating Polymers. 2. Linear Dynamics. *Macromolecules* **1998**, *31*, 1386−1397.
(55) Cui, G.; Boudara, V. A. H.; Huang, Q.; Baeza, G. P.; Wilson, A. J.; Hassager, O.; Read, D. J.; Mattsson, J. Linear Shear and Nonlinear Extensional Rheology of Unentangled Supramolecular Side-Chain Polymers. *J. Rheol.* **2018**, *62*, 1155−1174.
(56) Zhang, Z.; Liu, C.; Cao, X.; Gao, L.; Chen, Q. Linear Viscoelastic and Dielectric Properties of Strongly Hydrogen-Bonded Polymers near the Sol-Gel Transition. *Macromolecules* **2016**, *49*, 9192−9202.
(57) Wagner, M. H. Scaling Relations for Elongational Flow of Polystyrene Melts and Concentrated Solutions of Polystyrene in Oligomeric Styrene. *Rheol. Acta* **2014**, *53*, 765−777.
(58) Williams, M. L.; Landel, R. F.; Ferry, J. D. The Temperature Dependence of Relaxation Mechanisms in Amorphous Polymers and Other Glass-Forming Liquids. *J. Am. Chem. Soc.* **1955**, *77*, 3701−3707.
(59) Liu, C.-Y.; He, J.; Keunings, R.; Bailly, C. New Linearized Relation for the Universal Viscosity−Temperature Behavior of Polymer Melts. *Macromolecules* **2006**, *39*, 8867−8869.
(60) Semenov, A. N.; Rubinstein, M. Thermoreversible Gelation in Solutions of Associative Polymers. 1. Statics. *Macromolecules* **1998**, *31*, 1373−1385.
(61) Fetters, L. *Physical Properties of Polymers Handbook*; Mark, J. E., Ed.; Springer: New York, 2007.
(62) Rubinstein, M.; Colby, R. H. *Polymer Physics*; Oxford University Press: New York, 2003.
(63) Chen, Q.; Huang, C.; Weiss, R. A.; Colby, R. H. Viscoelasticity of Reversible Gelation for Ionomers. *Macromolecules* **2015**, *48*, 1221−1230.
(64) Rouse, P. E. A Theory of the Linear Viscoelastic Properties of Dilute Solutions of Coiling Polymers. *J. Chem. Phys.* **1953**, *21*, 1272−1280.
(65) Ferry, J. D. *Viscoelastic Properties of Polymers*, 3rd ed.; Wiley: New York, 1980.
(66) Baxandall, L. G. Dynamics of Reversibly Crosslinked Chains. *Macromolecules* **1989**, *22*, 1982−1988.
(67) Shabbir, A.; Javakhishvili, I.; Cerveny, S.; Hvilsted, S.; Skov, A. L.; Hassager, O.; Alvarez, N. J. Linear Viscoelastic and Dielectric Relaxation Response of Unentangled UPy-Based Supramolecular Networks. *Macromolecules* **2016**, *49*, 3899−3910.
(68) Van Steenberge, P. H. M.; Sedlacek, O.; Hernández-Ortiz, J. C.; Verbraeken, B.; Reyniers, M.-F.; Hoogenboom, R.; D'hooge, D. R. Visualization and Design of the Functional Group Distribution during Statistical Copolymerization. *Nat. Commun.* **2019**, *10*, 3641.
(69) Papagiannopoulos, A.; Fernyhough, C. M.; Waigh, T. A. The Microrheology of Polystyrene Sulfonate Combs in Aqueous Solution. *J. Chem. Phys.* **2005**, *123*, 214904.
(70) Panyukov, S. Loops in Polymer Networks. *Macromolecules* **2019**, *52*, 4145−4153.

https://doi.org/10.1021/acs.macromol.1c01908
Macromolecules 2022, 55, 928−941